DNS OF A TURBULENT BOUNDARY LAYER WITH SEPARATION

Michael Manhart
Fachgebiet Strömungsmechanik
Technische Universität München
85747 Garching, Germany
michael@flm.mw.tu-muenchen.de

Rainer Friedrich
Fachgebiet Strömungsmechanik
Technische Universität München
85747 Garching, Germany
r.friedrich@lrz.tu-muenchen.de

ABSTRACT

The present contribution reports on a direct numerical simulation (DNS) of a fully turbulent boundary layer that undergoes separation due to the presence of a pressure gradient at a moderate Reynolds number. The variation of the free-stream velocity has been chosen according to an experiment of Kalter and Fernholz (1994). Because of limited computational resources, the momentum thickness Reynolds number at the reference position is $Re_\theta = 870$ which is about half as large as that of the experiment. Nevertheless, a comparison of global values and first and second order statistics shows good agreement between simulation and experiment.

INTRODUCTION

The separation zone embedded in a turbulent flat plate boundary layer as a result of a streamwsie a pressure gradient is highly unsteady and characterized by low-frequency oscillations. The improvement of turbulence models in such flow regimes requires a deep understanding of the dynamics and mechanisms of separation and reattachment. DNS is a valuable tool to improve our physical insight because it provides accurate three-dimensional and time-dependent information of the flow variables. Up to now, only a limited number of direct numerical simulations of separated turbulent boundary layers are available. The separation of *turbulent* boundary layers is fundamentally different from that of laminar boundary layers that undergo transition between separation and reattachment.

The separation of a turbulent boundary layer has first been numerically analyzed by Coleman and Spalart (1993). Recently, Skote, et al. (2000) performed a DNS of a separated turbulent boundary layer. An extensive study has been performed by Na and Moin (1998) at a low Reynolds number ($Re_\theta = 300$, based on inlet free-stream velocity and momentum thickness). In their study, separation/reattachment have been enforced by strong adverse/favourable pressure gradients in streamwise direction.

The study presented here, is the first DNS that reproduces an actually performed experiment of a separated turbulent boundary layer (Kalter and Fernholz 1994). In comparison to Na and Moin's study, it has a significantly higher Reynolds number and the reattachment occurs in a region with vanishing pressure gradient instead of strong favourable pressure gradient. Therefore, Reynolds stresses play a crucial role in the momentum balance of the presented flow. This study aims at providing supplementary data for improving turbulence models and physical insight into the dynamics of separation and reattachment of this flow.

COMPUTATIONAL DETAILS

Our approach is based on a finite volume formulation of the incompressible Navier-Stokes equations on a staggered Cartesian non-equidistant grid. The spatial discretization is central and of second order for the convective and diffusive terms. For the time advancement of the momentum equation, an explicit second-order time step (leapfrog with time-lagged diffusion term) is used. The Poisson equation for the pressure is solved by a multi-

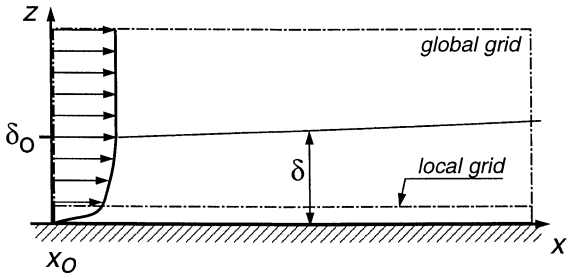

Figure 1: Geometry of the boundary layer simulations (not to scale).

grid method based on an iterative point-wise velocity-pressure iteration (Manhart 1999).

The code uses local grid refinement at the wall in order to save computational resources (Figure 1). The refinement of the local grids is achieved by dividing one coarse grid cell into 8 fine grid cells. The coarse and the fine grids are arranged in an overlapping way, so that the coarse grid is defined globally (global grid) and the fine grid is defined only locally (zonal grid). The coarse-grid and the fine-grid solutions are fully coupled. The coupling is achieved by transferring the fine-grid solution in the overlap region to the coarse grid. This so-called restriction is done at certain steps within the solution algorithm. We use averaging over four cell faces for the velocities and averaging over 8 grid cells for the pressure restriction (see Manhart 1998).

Periodic boundary conditions are prescribed in spanwise direction and no-slip at the wall. At the upper boundary of the domain, the vertical velocity is prescribed. At the outflow, a zero gradient condition is applied for the velocities. The time-dependent inflow profiles are constructed by superposition of a time-mean profile and fluctuation from a position $10\delta_0$ downstream (where δ_0 is the boundary layer thickness at the inlet plane). A detailed description of the boundary conditions is given in Manhart and Friedrich (1999).

The simulation is designed according to the experiment of Kalter and Fernholz (1994). In terms of boundary layer thickness at the inlet δ_0, the reference position in the simulation is located $10\delta_0$ downstream of the inlet (at $x/\delta_0 = 5.0$). Using the free-stream velocity U_0 at the inlet, the Reynolds numbers at this position are $Re_\theta = 870$ and $Re_\theta = 1560$ in the simulation and the experiment, respectively. In terms of the displacement thickness δ_r^* at the reference position, the dimensions of the computational box are $L_x = 542\delta_r^*$ in streamwise, $L_y = 128\delta_r^*$ in spanwise and $L_z = 54\delta_r^*$ in

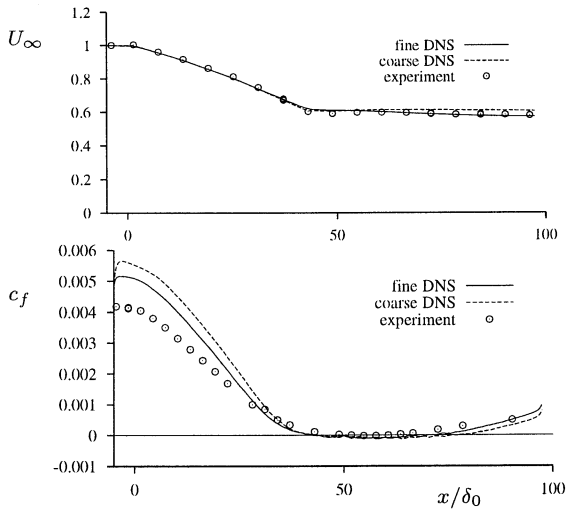

Figure 2: Distribution of free-stream velocity (top) and skin friction coefficient (bottom) in the separated turbulent boundary layer

vertical direction. In the following all quantities are normalized by U_0 and δ_0, respectively. ($\delta_r^*/\delta_0 = 0.188$).

We use $N_x \cdot N_y \cdot N_z = 1280 \cdot 448 \cdot 160$ grid cells for the global grid and $N_x \cdot N_y \cdot N_z = 1280 \cdot 896 \cdot 32$ grid cells for the zonal grid which covers only the first half of the computational domain. This leads to a grid resolution of $\Delta x^+ = 12.7$, $\Delta y^+ = 8.6$ and $\Delta z^+_{min} = 1.595$ at the wall. We performed a preliminary simulation, denoted here as "coarse DNS" (Manhart and Friedrich 1999), where the zonal grid extends from the inflow to the outflow plane. This simulation used a grid spacing of $\Delta x^+ = 26.4$, $\Delta y^+ = 12.4$ and $\Delta z^+_{min} = 3.3$. An analysis of the directional dissipation scale (see Manhart 2000) in this simulation revealed that the local grid is necessary only in the first half of the computational domain.

RESULTS

Global description

In Figure 2, the distributions of the free-stream velocity U_∞ and the skin friction coefficient c_f are shown. Since there is no variation of the free-stream velocity after separation ($x/\delta_0 \approx 40$), the boundary layer is slowly relaxing from the separated regime by diffusive and convective processes only. This leads to a long regime where c_f is nearly zero. The improvement of c_f by the use of a finer grid is clearly visible, especially in the initial regime where the adverse pressure gradient sets in. The remaining difference between DNS and experiment can be attributed to the different

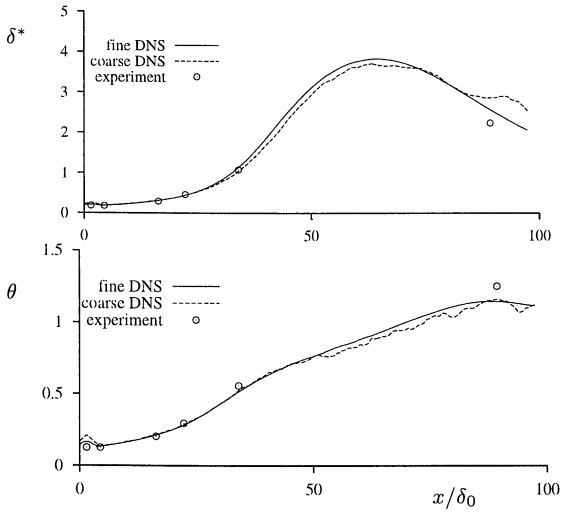

Figure 3: Displacement (top) and momentum (bottom) thickness in the separated turbulent boundary layer

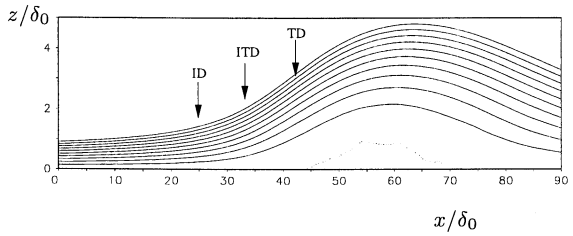

Figure 4: Streamlines of averaged velocity field

Reynolds numbers. Coles' empirical correlation (1962) gives values of $cf \approx 0.004$ for $Re_\theta = 1500$ which corresponds to the experiment and $cf \approx 0.0047$ for $Re_\theta = 870$ which corresponds to our DNS.

The displacements thickness δ^* and momentum thickness θ are shown in Figure 3. They are in good agreement with the experiment. The displacement thickness grows by a factor of about 20 during separation, which documents the need for a very large computational domain in wall-normal and spanwise direction.

The streamlines of the averaged velocity field in Figure 4 display the geometry of the separation bubble. According to the definition of Simpson (1996), the positions indicated in the Figure are incipient detachment (ID), intermittent transitory detachment (ITD) and transitory detachment (TD). TD (50% backflow in time) is at the same position as $\tau_w = 0.0$ which denotes detachment or separation (at $x/\delta_0 = 44$). The flow reattaches at $x/\delta_0 = 72$. The height of the separation bubble is about δ_0. Therefore, we can speak of a strong separation.

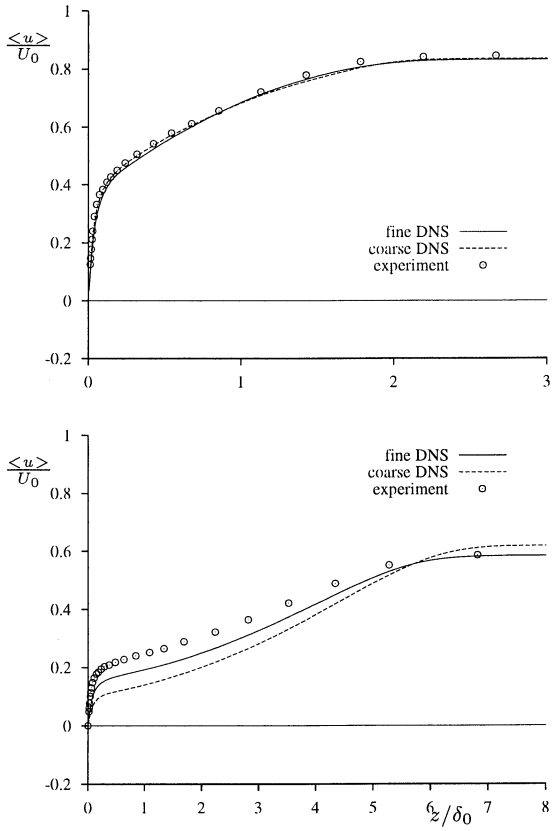

Figure 5: Averaged streamwise velocity profiles in comparison with the experiment of Kalter and Fernholz (1994); $x/\delta_0 = 22.17$ (top) and $x/\delta_0 = 90.0$ (bottom)

First- and second-order statistics

Velocity profiles averaged in time and spanwise direction are compared in Figure 5 at two different locations: one in the adverse pressure gradient region ($x/\delta_0 = 22.17$) and one after reattachment ($x/\delta_0 = 90.0$). In the separation zone, no experimental profiles are available. The coarse DNS has difficulties in the relaxation regime, where c_f relaxes too slowly. This is improved by the fine grid which shows better agreement with the experiment.

The same observation can be made in the RMS-value of the streamwise velocity component (Figure 6) which is significantly improved by the use of a finer computational grid. The RMS velocity fluctuation for the coarse DNS still shows a bump at the location of the zonal/global grid interface (at $z/\delta_0 = 0.44$). By the action of the pressure gradient, the peak of the RMS is reduced and moves away from the wall in accordance with the growth of the boundary layer thickness.

Momentum balance

In Figure 7 the momentum balance at a po-

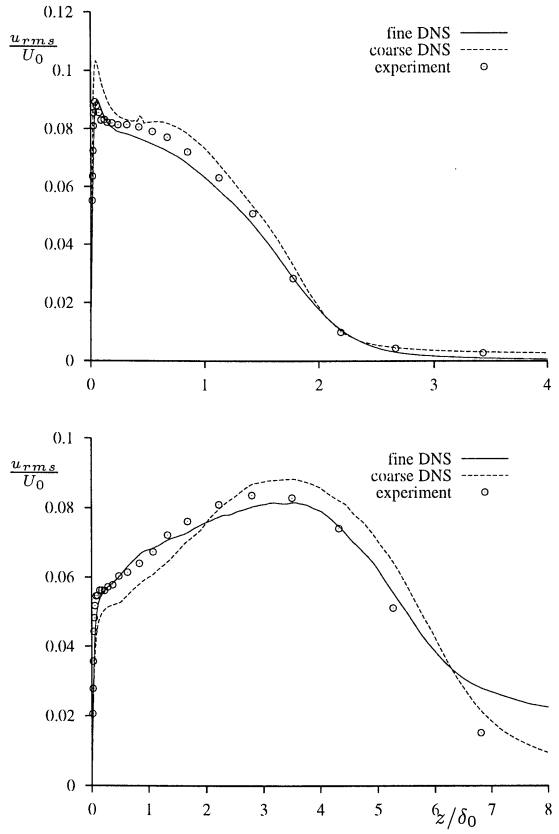

Figure 6: RMS of the streamwise velocity component in comparison with the experiment of Kalter and Fernholz (1994); $x/\delta_0 = 22.17$ (top) and $x/\delta_0 = 90.0$ (bottom)

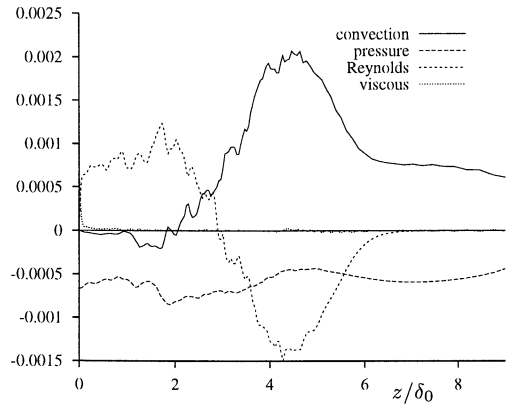

Figure 7: Momentum balance in the separation bubble ($x/\delta_0 = 50$)

sition $x/\delta_0 = 50$ is shown. The pressure term is nearly constant throughout the whole layer. In the shear layer above the separation region ($3 \leq z/\delta_0 \leq 6$), the convection term gives a positive contribution and balances the sum of the pressure term and the Reynolds term. The latter extracts a significant amount of momentum from the shear layer and brings it down to the separation bubble where it is balanced with the pressure term. At this streamwise position, the viscous term is negligible and the Reynolds term is the only mechanism which accelerates the flow near the wall and acts against the separation.

Instantaneous structure of the separation bubble

The separation and reattachment lines are not fixed in space and time. In order to get an impression of the complicated nature of the instantaneous shape of the separation bubble, we show a perspective view of the streamwise velocity component in Figure 8 and a top view of the isosurface of $u = 0.0$ in Figure 8. The main feature emanating from the two pictures is the highly irregular shape of the separation bubble. At the instant shown, the separation line meanders between $x/\delta_0 = 40$ and $x/\delta_0 = 50$ with a dominant spanwise wavelength of $5\delta^*$ (in terms of local displacement thickness). Also, there are small forward flow regions embedded completely in the separation bubble.

The 2D roll-up process of the shear layer plays an important role in the overall dynamics of the separation bubble showing an oscillatory behaviour of growth and sudden collapse (see also Na and Moin 1998). This process is illustrated in Figure 9, where the spanwise averaged streamwise velocity component is displayed for different time steps. The separation bubble is growing until a certain streamwise extent is reached ($tU_\infty/\delta_0 = 2397$). Then the downstream part of it slowly looses thickness simultaneously over a long streamwise distance. Finally, the reverse flow disappears between $x/\delta_0 = 65$ and $x/\delta_0 = 80$ within a very short time.

CONCLUSIONS

We have performed a DNS of a fully turbulent flat plate boundary layer with separation as a result of a streamwise pressure gradient. After reattachment, the boundary layer slowly relaxes without acceleration of the free-stream flow. To our knowledge, this is the first DNS of such a flow performed to date which is comparable to a real experiment. The accordance with the experiment is fully satisfying. The momentum balance in the separated region is strongly governed by Reynolds stresses. The separation bubble shows a complicated spatial structure including large-scale variations in spanwise direction. Time sequences of spanwise averaged velocity fields demonstrate the

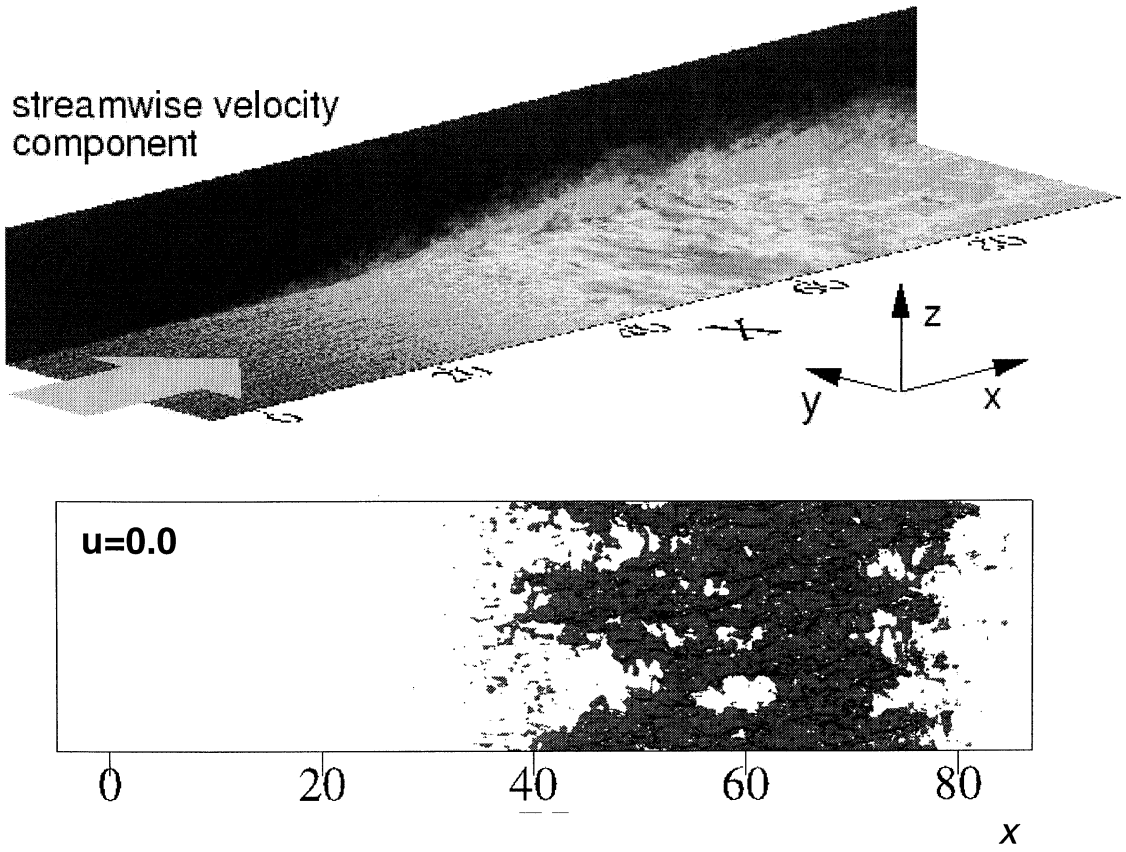

Figure 8: Instantaneous velocity fields: perspective view of streamwise velocity component (top);Top view of isosurface $u = 0.0$ of streamwise velocity component

flapping of the separation bubble, observed also in other experiments and simulations.

*

References

Coleman, G. and Spalart, P. (1993). Direct numerical simulation of a small separation bubble. In Speziale, C. and Launder, B., eds., *Near-Wall Turbulence Flows*, pp. 277–286. Elsevier.

Coles, D. (1962). The turbulent boundary layer in a compressible fluid. In *Report R-403-PR*. The Rand Corporation, Santa Monica, CA.

Kalter, M. and Fernholz, H. (1994). The influence of free-stream turbulence on an axisymmetric turbulent boundary layer in, and relaxing from, an adverse pressure gradient. In *5. European turbulence conference, Siena 1994*.

Manhart, M. (1998). Zonal direct numerical simulation of turbulent plane channel flow. In Friedrich, R. and Bontoux, P., eds., *Computation and visualization of three-dimensional vortical and turbulent flows. Proceedings of the Fifth CNRS/DFG Workshop on Numerical Flow Simulation*, volume 64 of *Notes on Numerical Fluid Mechanics*. Vieweg Verlag.

Manhart, M. (1999). Direct numerical simulation of turbulent boundary layers on high performance computers. In Krause, E. and Jaeger, W., eds., *High performance Computing in Science and Engineering 1998*. Springer Verlag.

Manhart, M. (2000). The directional dissipation scale: a criterion for grid resolution in direct numerical simulations. In Dopazo et al., eds., *Advances in Turbulence VIII*, pp. 667–670, Barcelona. Eigth European Turbulence Conference, CIMNE.

Manhart, M. and Friedrich, R. (1999). Towards DNS of separated turbulent boundary lay-

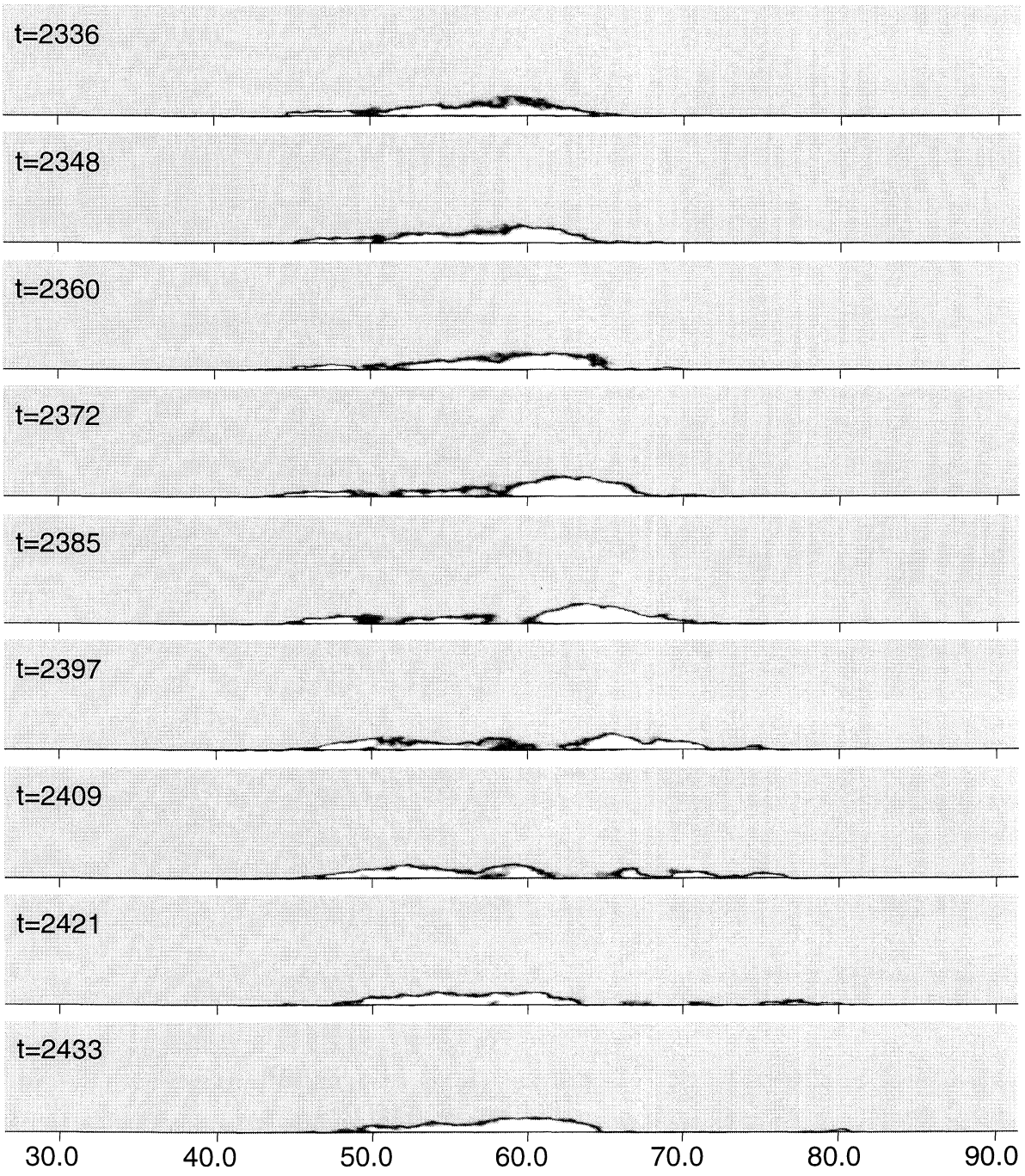

Figure 9: Spanwise averaged streamwise velocity component; dark gray is from $-0.01 < u < 0.0$

ers. In Voke, P., Sandham, N., and Kleiser, L., eds., *Direct and Large-Eddy Simulation III*, pp. 429–440. Kluwer Academic Publishers, Dordrecht.

Na, Y. and Moin, P. (1998). Direct numerical simulation of a separated turbulent boundary layer. *J. Fluid Mech.*, **370**, 175–201.

Simpson, R. (1996). Aspects of turbulent boundary-layer separation. *Prog. Aerospace Sci.*, **32**, 457–521.

Skote, M., Henningson, D., Hirose, N., Matsuo, Y., and Nakamura, T. (2000). Parallel DNS of a separating turbulent boundary layer. In *Proceedings of the Parallel CFD 2000*, Trondheim, Norway. NTNU.